Journal of Materials and Environmental Science
ISSN : 2028-2508
e-ISSN : 2737-890X
CODEN : JMESCN

J. Mater. Environ. Sci., 2026, Volume 17, Issue 6, Page 1036-1046

http://www.jmaterenvironsci.com

Tensoactive and Ripening Effects in the Formation of ZnO Nanoparticles under Varied Aqueous Synthesis Conditions

González-Hurtado M. [1], George-Ponce de León G. [1], Alimonta-Álvarez A. [1], Fernández-Sánchez P. [2], Iribarren A. [1]*

[1] *Instituto de Ciencia y Tecnología de Materiales, Universidad de La Habana, Zapata s/n, esq. G, Vedado, Plaza, La Habana 10400, Cuba.*
[2] *Departamento de Física de Materiales, Facultad de Ciencias Físicas, Universidad Complutense de Madrid, 28040 Madrid, España*

Corresponding author. Email addresses: augusto.iribarren@gmail.com, augusto@imre.uh.cu

Received *03 May 2026,*
Revised *22 June 2026,*
Accepted *23 June 2026*

Keywords:
- ✓ *ZnO nanoparticles;*
- ✓ *aqueous synthesis;*
- ✓ *crystallite size;*
- ✓ *Strain*

Citation: *Gonzalez-Hurtado M., George-Ponce de León G., Alimonta-Álvarez A., Fernández-Sánchez P., Iribarren A. (2026) Tensoactive and Ripening Effects in the Formation of ZnO Nanoparticles under Varied Aqueous Synthesis Conditions, J. Mater. Environ. Sci., 17(6), 1036-1046*

Abstract: The aim of this study is to explore the size and structural behavior of ZnO nanoparticles obtained by aqueous synthesis under varied conditions. Three aqueous synthesis routes were employed to obtain ZnO nanoparticles (ZnO NPs): a standard method with mechanical stirring (ZnO-std), a polyvinyl alcohol–assisted route (ZnO-PVA), and a high-speed stirring variant (ZnO-UT). ZnO-std produced particles with an average grain size of 87 nm. ZnO-PVA yielded the smallest particles (~73 nm) with reduced lattice constants and tensile strain, effects attributed to the surfactant action of PVA during nucleation. In contrast, ZnO-UT generated the largest particles (~92 nm) with compressive strain and the lowest lattice constant, consistent with Ostwald ripening driven by strong stirring. These findings highlight how surfactant mediation and stirring dynamics govern ZnO nanostructure evolution, providing a basis for tailoring particle size and strain in functional applications.

1. Introduction

In recent decades, nanodimensioned materials have gained significant relevance and become the focus of extensive research (Malik *et al.* 2023, Kolahalam *et al.* 2019). Nanomaterials are generally defined as materials with dimensions of approximately 100 nm or less in at least one geometric direction. They exhibit remarkable and unique physical and chemical properties, which depend on factors such as shape, size, charge distribution, and structural order (Zafar *et al.* 2022). Consequently, numerous studies have sought to modify and control these characteristics. Among these, nanoparticle shape and size are particularly influential in determining material properties (Roduner 2026), leading to the development of multiple synthesis methods for nanomaterials (Baig *et al.* 2021).

Nanomaterials can be classified into several categories, including carbon-based, metals, metal oxides, semiconductors, ceramics, and other nanoparticles and nanostructures (Hassan, 2015; Tabaght *et al.*, 2021; Salem *et al.*, 2022; Hossain *et al.*, 2023; El Garrab & Zekriti, 2025; Mohamed *et al.*, 2025). Within this broad spectrum, inorganic oxides—especially those of transition metals—stand out due to

their exceptional properties and wide-ranging applications in sensors, optoelectronics, photovoltaics, electrochemistry, photocatalysis, energy storage, and biomedicine (Saidi *et al.*, 2022; Xiong *et al.*, 2022; El Garrab & Zekriti, 2024; Abouri *et al.*, 2025; Husaini, 2026). Among transition-metal oxides, zinc oxide (ZnO) occupies a prominent position.

ZnO continues to attract research interest due to its well-established, enhanced, and emerging applications across diverse scientific and technological fields (Clarke and Ghandi 2023, Islam *et al.* 2025; Alshahateet *et al.*, 2024; Dey *et al.* 2025, Ragu Prasath *et al.* 2026). It is an n-type semiconductor with high conductivity, a band gap energy of 3.37 eV (rendering it transparent to visible light), and an exciton binding energy of 60 meV—significantly higher than the thermal energy at room temperature (Ong *et al.* 2018, Morkoç and Özgür 2009, Wang 2009, Ghamarpoor *et al.* 2024).

A wide variety of synthesis methods have been employed to obtain ZnO, each producing distinct morphologies with specific properties (Garner *et al.* 2023, Leung *et al.* 2004, Abd Alsaheba *et al.* 2025). Among these, nanosized morphologies (Saeed *et al.* 2023), particularly nanoparticles (NPs) (Jiang *et al.* 2023, Shaba *et al.* 2021, Droepenu *et al.* 2022), have been extensively studied. Techniques such as aqueous synthesis, hydrothermal growth, and chemical decomposition are commonly used (Iribarren *et al.* 2019, Iribarren *et al.* 2014, Dem'Yanets *et al.* 2006). The characteristics of ZnO NPs depend strongly on the synthesis method, even when methods appear similar. Therefore, it is crucial to elucidate the properties of samples obtained by related approaches. Previous studies have also explored the use of complexing agents to modify the physical properties of ZnO NPs (Bezerra *et al.* 2019, Soli *et al.* 2021).

In this work, ZnO nanoparticles (ZnO NPs) were synthesized through modified aqueous routes to probe the influence of surfactant mediation and stirring dynamics. Specifically, polyvinyl alcohol (PVA), which is is a water-soluble polymer (Agrawal *et al.* 2023), was incorporated into the precursor solution and high velocity stirring was applied as a process variation to a previously reported method (Iribarren *et al.* 2019). The resulting ZnO NPs were systematically compared formorphological and structural characteristics, revealing distinct size and strain profiles attributable to surfactant effects and energy transfer during nucleation. These insights establish a framework for tailoring ZnO nanostructures via synthesis parameters, enabling informed selection for optoelectronic and energy-related applications.

2. Methodology

2.1 Experiments

For two of the synthesis a MC-8 Bunsen Magnetic Stirrer with Heating was used. The third synthesis was carried out with a Homogenizer IKA T 25 digital ULTRA-TURRAX. The annealing of the obtained nanoparticles was made in a Mufla Furnance SX2-12TP.

A scanning electron microscopy (SEM) Tescan, Type Vega 3 SBH instrument with a previous 1.3 nm Au coating of the samples was used to obtain the nanoparticle morphologies. Structural analysis was carried out with a Bruker D-8 Advance x-ray diffractometer and CuKα radiation (λ=0.15406 nm) and incidence geometry of grazing and a beam incidence angle of 1° and recorded in steps of 0.02 for 3 s.

2.2 Synthesis methods

For the obtaining of ZnO NPs three methods with specific changes were used. One of them was considered as reference and it is name "standard" synthesis method (ZnO-std) using a hot plate with stirring of the precursor dissolution. A second method was similar to the ZnO-std method, but with addition of polyvinyl alcohol (ZnO-PVA). The third method was using a Ultra-TURRAX homogenizer for stirring the precursor dissolution (ZnO-UT). Following, a detailed description of the methods is presented. After obtaining the ZnO NPs, they were put under thermal treatment in air at 400°C for 3 hours.

2.2.1 "Standard" synthesis method (ZnO-std)

This method has been usual in previous works (Iribarren *et al.* 2019). The standard synthesis method (ZnO-std) has been described elsewhere (Iribarren *et al.* 2019). A dissolution was prepared with an amount of 5 g of Zn acetate ($Zn(CH_3CO_2)_2 \bullet 2H_2O$, $ZnAc_2$), which was dissolved in 20 mL of bidistilled H_2O under magnetic stirring at 60°C. Dissolution of 1 g NaOH in 20 mL of bidistilled water was prepared and added by slow dropping to the ZnAc2 dissolution under stirring at 60°C, which was kept for 2 more hours. A white precipitation was observed. The resulting dissolution with the precipitation was kept at rest for 72 hours and then was centrifuged at 9000 rpm for 30 min alternating twice with successive washes in 20 mL of ethanol and in 20 mL of distilled water. After decanting, the obtained powder remained drying at room environment for 48 hours.

2.2.2 PVA-added synthesis method (ZnO-PVA)

Dissolution of 1 g of PVA (average m. w. 155 000) in 20 mL of bidistilled water under stirring at around 85°C up to total dissolution was prepared. The ZnO synthesis procedure was similar to that of ZnO-std, but 1 mL of the 1PVA:20H_2O dissolution was added to the $ZnAc_2$+H_2O dissolution. The same steps of NaOH dissolution dropping, washing, centrifugation and drying were followed up to obtaining a white powder.

2.2.3 UltraTurrax-assisted synthesis method (ZnO-UT)

Similar procedure to that of the ZnO-std method was used, but the stirring was carried out with a Utra-Turrax homogenizer at 5700 rpm and 60°C. After dropping of the NaOH dissolution the stirring was increased up to 9800 rpm. The rest of steps, i. e., centrifugation and drying, were followed up to obtaining a white powder, were followed as in the ZnO-std method.

2.2.4 Annealing

All the samples were annealed at the same time, according to a procedure previously established (Iribarren *et al.* 2019), in a furnace at 400°C for 3 h, in order to eliminate undesirable organic residuals.

3. Results and Discussion

3.1 Morphological analysis

The analysis of SEM images of **Figure 1** indicates that all the nanoparticles are spheroidal forming agglomerations, although the NPs of **Figure 1b** obtained with the ZnO-PVA method are seen smaller and in **Figure 1c** the NPs obtained with the ZnO-UT method are observed larger. The measurement of the grain sizes D_{SEM} and the average volume of the grains V_{SEM}, which was estimated with the sphere volume equation, are presented in **Table 1**.

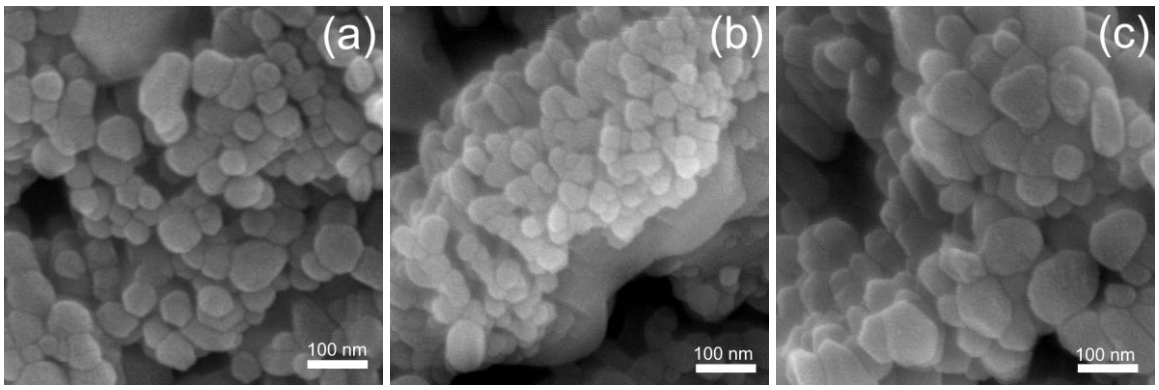

Figure 1. SEM images of the ZnO NPs obtained with the ZnO-std (a), the ZnO-PVA (b) and ZnO-UT (c) methods

Table 1. Sizes and volumes of the grains for each method.

Method	D_{SEM} (nm)	V_{SEM} (nm^3)
ZnO-std	87±5	344791 (±17%)
ZnO-PVA	73±6	203689 (±25%)
ZnO-UT	92±5	407720 (±16%)

3.2 Structural analysis

From **Figure 2** that displays the diffractograms of ZnO NPs obtained with each synthesis method, it is possible to observe that in all the samples only peak corresponding to single-phase wurtzite hexagonal are present as observed in comparison with the ZnO pattern (JCPDS 2003). The angle of the main peaks increases according the synthesis method as observed in **Table 2**.

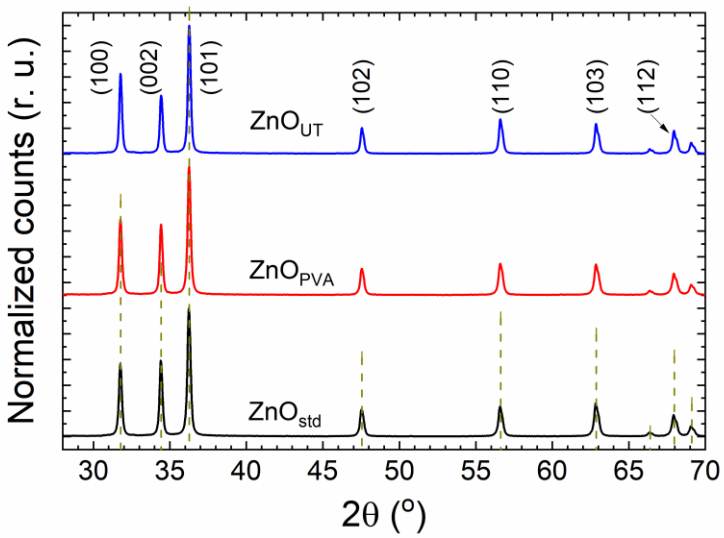

Figure 2. Diffractograms of the ZnO NPs obtained with the three synthesis methods

It means that the lattice of the NPs obtained with the ZnO-std method is the most tensed, those NPs obtained with ZnO-PVA one is less tense and those obtained with ZnO-UT is the less tense. Correspondingly, using the expression (Cullity 1956):

$$sin^2\theta = \frac{\lambda^2}{4}\left[\frac{4}{3}\times\frac{(h^2+hk+k^2)}{a^2}+\frac{l^2}{c^2}\right] \qquad \textbf{Eqn. 1}$$

where θ is the peak angle, λ=0.15405 nm x-ray wavelength, and h, k and l are the Miller indexes, the lattice constants a=b and c were calculated using the peaks (100) and (002) as tabulate in the Table 1 and plotted in **Figure 3**. The macrostrains over the directions a and c were calculated in comparison with the pattern (JCPDS 2003) with the expressions:

$$\delta_a = \frac{a-a_0}{a_0} \text{ and } \delta_c = \frac{c-c_0}{c_0}. \qquad \textbf{Eqn. 2}$$

where a_0 and c_0 are the pattern lattice parameter. The volume of the unit cell V_c in an hexagonal lattice, as obtained with the expression (Cullity 1956):

$$V_c = \frac{\sqrt{3}a^2c}{2} = 0.866a^2c \qquad \textbf{Eqn. 3}$$

The average number of unit cells (n_c) in the grains was calculated from the relationship between V_c and V_{SEM} and it is also presented in **Table 2** and it is plotted in **Figure 4**.

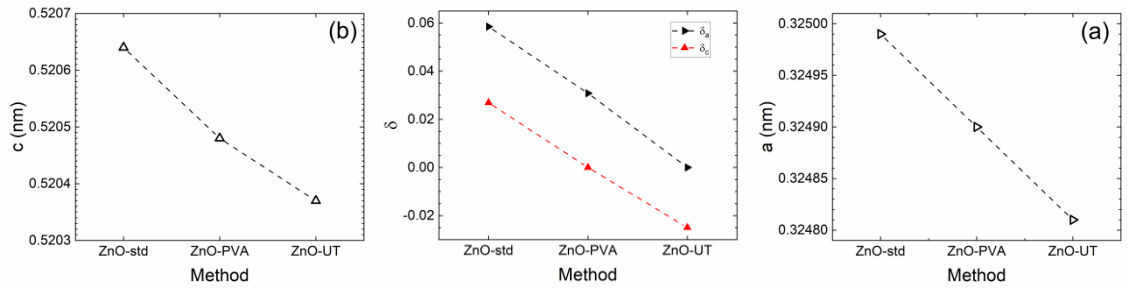

Figure 3. Behavior of the lattice parameters a and c and macrostrain δ for the crystallographic directions with each synthesis method.

Table 2. 2θ angles, lattice parameters a and c, macrostrains δ over the crystallographic planes, volume of the unit cell of ZnO NPs V_c and average number of unit cells in the grains n_c obtained with the three synthesis methods.

Method	$2\theta_{(100)}$ (°)	$2\theta_{(002)}$ (°)	a (nm)	δ_a (%)	c (nm)	δ_c (%)	V_c (nm^3)	n_c ($\times 10^6$)
Pattern	31.7790	34.430	0.3248	-	0.5205	-	0.04755	-
ZnO-std	31.7660	34.421	0.3250	0.0616	0.5206	0.0192	0.04762	7.24
ZnO-PVA	31.7745	34.432	0.3249	0.0307	0.5205	~0	0.04758	4.28
ZnO-UT	31.7834	34.440	0.3248	~0	0.5204	-0.0192	0.04754	8.58

As observed from the angular position of the (100) and (002) peaks the ZnO NPs obtained with the ZnO-std method is tensed in comparison to the pattern, but the tension decreases for NPs obtained from the ZnO-PVA method and becomes compressive for those with the ZnO-UT one, as can be also observed from the macrostrain tabulated in **Table 2** and plotted in **Figure 3c**. Those behaviors correspond with the decreasing of the lattice constants as in **Figures 3a** and **3b**. On the other hand, the number of unit cells decreases for the NPs with the ZnO-PVA method respect to those of ZnO-std one and increases for those with the ZnO-UT one, which was plotted in **Figure 4**.

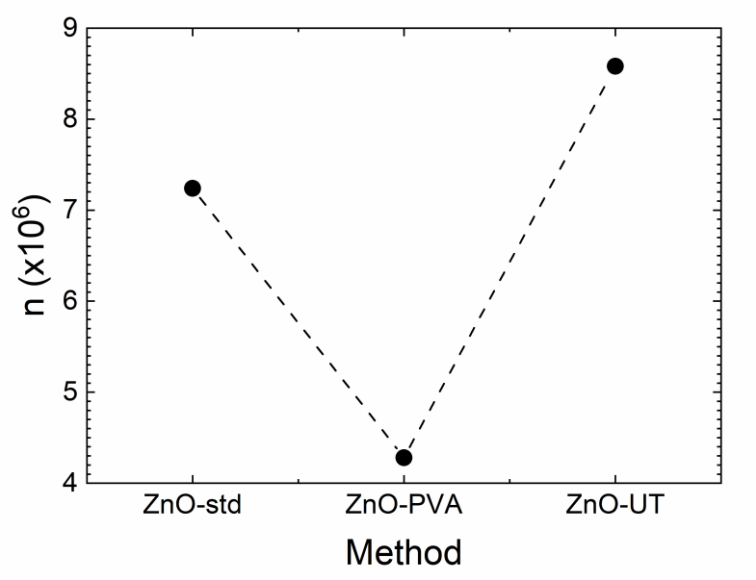

Figure 4. Average number of unit cells in the grains.

The crystallite sizes and effective microstrain distribution of the NPs from diffractograms were calculated by pseudoVoig fitting of the peaks and using the Williamson-Hall expression (Williamson and Hall 1953), given by:

$$w\ cos\theta = \frac{\lambda}{D} + 4\varepsilon_c sin\theta \qquad \textbf{Eqn 4}$$

where w is the full width at half maximum, D is the crystallite size (volume average), and ε_c is the effective microstrain distribution. Six peaks were used for using the Willimason-Hall expression.

On the ther hand, for determining the crystallite size and strain distribution in a specific plane a Voigt fitting, that gives Lorentzian and Gaussian components. Crystallite size was estimate with the parameters of the Lorentzian component using the Scherrer expression (Mittemeijer and Welzel 2013):

$$d_{Sch} = \frac{0.9\,\lambda}{w_L \cos\theta} \qquad \textbf{Eqn 5}$$

where w_L is the Lorentzian full width at half maximum, λ is the wavelength of x-ray radiation, and θ the angle of the corresponding peak (hkl) of the Bragg reflection. The microstrain distribution was estimate from the parameters of the Gaussian component and using the Stokes-Wilson expression (Stokes and Wilson 1944):

$$\mu_\varepsilon = \frac{w_G}{2tan\theta} \qquad \textbf{Eqn 6}$$

where w_G is the Gaussian full width at half maximum in the Voigt fitting of the diffraction peak (hkl). For all these analysis we used the main peaks of the diffractograms, i. e., (100), (002) and (101). **Table 3** tabulates the crystallite sizes D_{WH} and effective microstrains distribution ε_{WH} from Williamson-Halls expressions, crystallite sizes D_{Sch} of the main peaks using Scherrer expression, and microstrain distributions by crystallographic planes μ_ε from Stokes-Wilson expression of the ZnO NPs obtained with each synthesis method.

Table 3. Crystallite sizes D_{WH} and effective microstrain distribution ε_{WH} from Williamson-Halls expressions, crystallite sizes D_{Sch} of the main peaks using Scherrer expression, and microstrain distributions for crystallographic direction μ_ε from Stokes-Wilson expression of the ZnO NPs.

Sample	D_{WH} (nm)	ε_{WH} (%)	Peak (100)		Peak (002)		Peak (101)	
			D_{Sch} (nm)	μ_ε (%)	D_{Sch} (nm)	μ_ε (%)	D_{Sch} (nm)	μ_ε (%)
ZnO-std	91.6±0.5	0.75	71.0	0.22	79.2	0.21	73.5	0.21
ZnO-PVA	78.5±0.3	0.64	73.2	0.21	84.7	0.21	74.1	0.21
ZnO-UT	87.4±0.3	0.62	87.2	0.21	106.1	0.23	89.9	0.20

The grain and crystallite sizes obtained from SEM images and Williamson-Hall expression are near for the three synthesis methods respectively as observed in **Figure 5a**. That indicates that in average each grain is practically formed by one crystallite. However, it is possible to observe that there is preferential distortion on the (002) plane in the ZnO NPs obtained with the ZnO-PVA method and it is more accented in those with the ZnO-UT method. In SEM image of **Figure 1c** it is possible to observe the ellipsoidal form of the grains, which is related to that preferential crystallite size in the (002) direction. The effective microstrain distribution ε_{WH} decreases with the ZnO-PVA and ZnO-UT methods as displayed in **Figure 5b**. The microstrain distributions for all the methods and planes are near and can be considered with an average $\mu_\varepsilon \cong 0.21\%$.

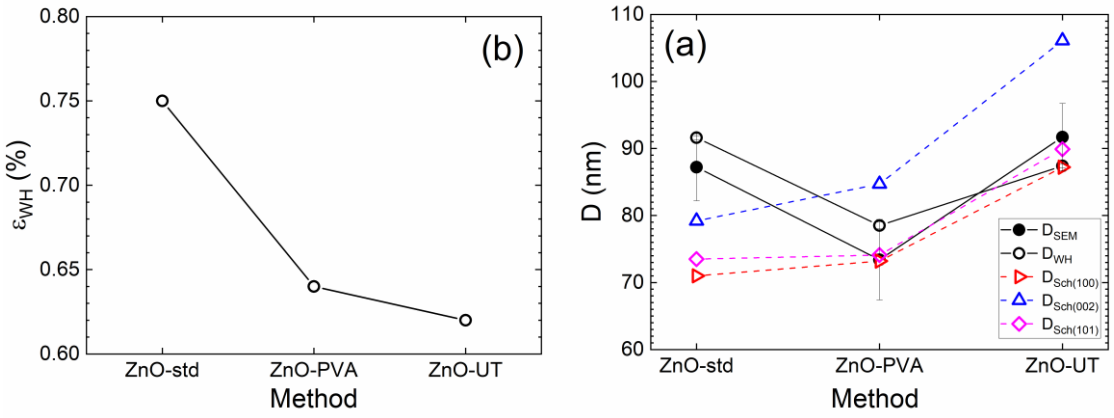

Figure 5. Grain (D_{SEM}) and crystallite sizes (a) and effective microstrain distribution (b) as functions of the synthesis method.

In other analysis of the diffractograms, the crystallographic texture or intensity correlation of each hkl peak Ip_{hkl} can be found with the expression:

$$Ip_{hkl} = \frac{I_{hkl}}{\sum_n I_{hkl}} \qquad \textbf{Eqn 7}$$

where I_{hkl} is the intensity of each (hkl) peak and n is the number of peaks used. We used the three most intense peaks, which are those of the planes (100), (002) and (101), i. e., n=3.

Figure 6 shows a comparison of the texture for the three choose peaks in the three obtaining methods and the texture values of the pattern are also shown. It is possible observe that each method influences differently on the texture. That is related to changes in the preferential growth of each plane. The texture given by the (100) peak is around that of the pattern for all the obtaining methods. The texture of the

(002) peak is higher than that of the pattern for the ZnO-std and ZnO-PVA synthesis, but it is near that of the pattern for the ZnO-UT synthesis.

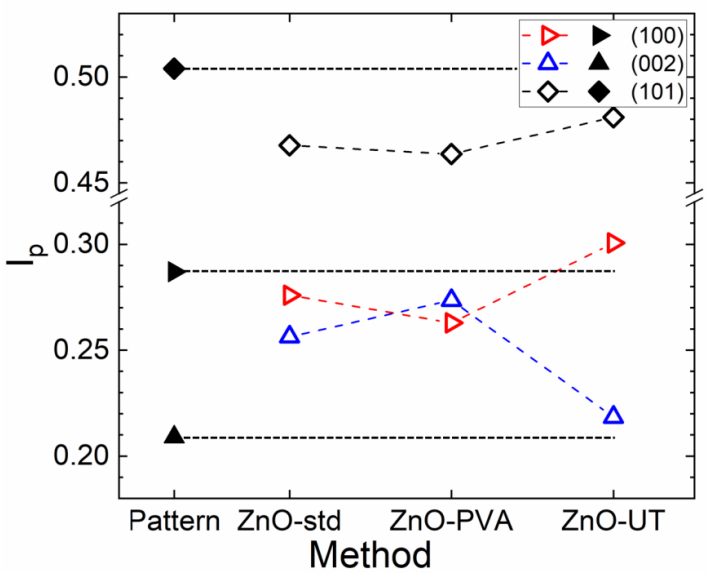

Figure 6. Behavior of the relative intensities I_p of the main peaks for each method. The solid symbols correspond to the relative intensities of the ZnO pattern.

The results indicate that the incorporation of PVA reduces grain size, suggesting its potential for grain-size control in ZnO nanoparticle synthesis. This reduction is attributed to the tensoactive effect of PVA (Cortes *et al.* 2021)] during nucleation and growth. In contrast, the ZnO-UT method produced a slight increase in average grain size. Although high-speed stirring is often associated with grain refinement, in this case Ostwald ripening (Hachem *et al.* 2022) and the additional energy supplied by strong stirring appear to dominate over shear effects, leading to grain growth and improved structural organization. The lattice constants (a and c) decreased for ZnO-PVA relative to ZnO-std, with the lowest values observed in ZnO-UT. Similarly, microstrain was reduced in ZnO-PVA and reached its lowest level in ZnO-UT compared to ZnO-std. Furthermore, ZnO-UT nanoparticles exhibited textures of the three main diffraction peaks approaching those of the reference pattern, whereas ZnO-std and ZnO-PVA showed deviations. These findings highlight the distinct roles of surfactant mediation and stirring dynamics in controlling grain size, strain, and crystalline texture in ZnO nanostructures.

Conclusion

ZnO nanoparticles (ZnO NPs) were synthesized through three aqueous routes: a standard method with mechanical stirring (ZnO-std), a polyvinyl alcohol–assisted method (ZnO-PVA), and a high-speed homogenizer variant (ZnO-UT). Comparative analysis revealed that PVA addition produced smaller grains and crystallites with reduced strain and lower lattice constants, effects attributed to the surfactant action of PVA during nucleation. In contrast, the ZnO-UT method yielded larger grains with crystallites comparable to ZnO-std but exhibiting the lowest strain and disorder, consistent with energy transfer and Ostwald ripening under strong stirring. These findings demonstrate that surfactant mediation and stirring dynamics critically govern ZnO nanostructure evolution, providing a basis for tailoring particle size, strain, and structural order to optimize performance in functional applications.

Acknowledgement. The authors acknowledge Mario Herrera, Oswaldo Gomez, Daniel Aguilar and Román Castro from CINVESTAV-Merida, Mexico, and to Nicolas Sargado from IMRE-UH, Cuba for technical

support. The authors also thank to Dr. Patricia Quintana for the XRD measurements in LANNBIO of Conacyt Fomix-Yucatán. This work is under the project PN223LH008-66 from the National Program of Nanoscience and Nanotechnology (PN3) and the project PN223LH010-58 from the National Program of Basic and Natural Sciences (PNCBN), Cuba.

Disclosure statement: *Conflict of Interest:* The authors declare that there are no conflicts of interest.
Compliance with Ethical Standards: This article does not contain any studies involving human or animal subjects.

References

Abd Alsaheba R.A., Rahimnejad M., Atyia M.A. (2025) Exploring Preparation of Zinc Oxide Nanoparticles Synthesis Mechanisms and Applications: A Comprehensive Review, *IJE Transactions B: Applications* 38(05), 1223-1244. https://doi.org/10.5829/ije.2025.38.05b.21

Abouri, M., Benzaouak, A., Elouardi, M., El Hamdaoui L., Zaaboul F., Azzaoui K., Hammouti B., Sabbahi R., Jodeh S., El Belghiti M. A. & El Hamidi A. et al. (2025). Enhanced photocatalytic degradation of Rhodamine B using polyaniline-coated XTiO3(X = Co, Ni) nanocomposites. *Scientific Reports*, 15, 3595. https://doi.org/10.1038/s41598-024-83610-1

Agrawal P. K., Sharma P., Singh V. K., Chauhan S. (2023) A Comprehensive Review on the Engineering of Biocompatible Polyvinyl Alcohol Composites with Enhanced Properties Using Carbonaceous Fillers, *J. Mater. Environ. Sci.* 14(5), 560-581.

Alshahateet S.F., Altarawneh R.M., Al-Tawarh W.M., Al-Trawneh S.A., Al-Taweel S., Azzaoui K., Merzouki M., Sabbahi R., Hammouti B., Hanbali G., Jodeh S. (2024). Catalytic green synthesis of Tin(IV) Oxide nanoparticles for phenolic compounds removal and molecular docking with EGFR Tyrosine Kinase, *Scientific reports*, 14(1), 6519, https://doi.org/10.1038/s41598-024-55460-4

Baig N., Kammakakam I., Falath W. (2021) Nanomaterials: a review of synthesis methods, properties, recent progress, and challenges, *Mater. Adv.* 2(6), 1821-1871. https://doi.org/10.1039/D0MA00807A

Bezerra J. B., Matos R. S., Zucolotto B., Pedra P. P., Ferreira N. S. (2019) Effects of different complexing agents on the physical properties of ZnO nanoparticles, *Mater. Sci. Tech.-Lond* 35(2), 231-239. https://doi.org/10.1080/02670836.2018.155

Clarke B., Ghandi K. (2023) The Interplay of Growth Mechanism and Properties of ZnO Nanostructures for Different Applications, *Small* 19(44), 2302864. https://doi.org/10.1002/smll.202302864

Cortés H., Hernández-Parra H., Bernal-Chávez S. A., Del Prado-Audelo M. L., Caballero-Florán I. H., Borbolla-Jiménez F. V., González-Torres M., Magaña J. J., Leyva-Gómez G. (2021) Non-Ionic Surfactants for Stabilization of Polymeric Nanoparticles for Biomedical Uses, *Materials* 14(12), 3197. https://doi.org/10.3390/ma14123197

Cullity B. D. (1956) *Elements of X-ray Diffraction*, Massachusetts, USA: Addison-Wesley Publishing Company, Inc.

Dem'Yanets L. N., Li L. E. and Uvarova T. G. (2006) Zinc oxide: hydrothermal growth of nano and bulk crystals and their luminescent properties, *J. Mater. Sci.* 41(5), 1439–1444. https://doi.org/10.1007/s10853-006-7457-z

Dey S., Iochan Mohanty D., Divya N., Bakshi V., Mohanty A., Rath D., Sabui R. (2025). A critical review on zinc oxide nanoparticles: Synthesis, properties and biomedical applications, *Intelligent Pharmacy* 3(1), 53-70. https://doi.org/10.1016/j.ipha.2024.08.004

Droepenu E. K., Wee B. S., Chin S. F., Kok K. Y., Maligan M. F. (2022) Zinc Oxide Nanoparticles Synthesis Methods and its Effect on Morphology: A Review, *Biointerface Research in Applied Chemistry* 12, 4261 - 4292. https://doi.org/10.33263/BRIAC123.42614292

El Garrab C., Zekriti M. (2024). Numerical investigation of SERS effects of silver dimers based on homo and hybrid nanoparticles, *Physica B: Condensed Matter*, 686, 416071, ISSN 0921-4526, https://doi.org/10.1016/j.physb.2024.416071

El Garrab M. and Zekriti M. (2025). Tuning sensitivity and limit of detection of nanoparticle dimer based on SiO2@Au core-shell for breast cancer diagnosis and prediction of treatment benefit, *Med. Eng. Phys*. 146, 104437 https://doi.org/10.1016/j.medengphy.2025.104437

Gartner M., Stroescu H., Mitrea D., Nicolescu M. (2023) Various Applications of ZnO Thin Films Obtained by Chemical Routes in the Last Decade, *Molecules* 28, 4674. https://doi.org/10.3390/molecules28124674

Ghamarpoor R., Fallah A., Jamshidi M. (2024) A Review of Synthesis Methods, Modifications, and Mechanisms of ZnO/TiO_2-Based Photocatalysts for Photodegradation of Contaminants, *ACS Omega* 9, 25457−25492. https://doi.org/10.1021/acsomega.3c08717

Hachem, K., Ansari, M.J., Saleh, R.O., Kzar, H.H., Al-Gazally, M.E., Altimari, U.S., and Kianfar, E. (2022). Methods of chemical synthesis in the synthesis of nanomaterial and nanoparticles by the chemical deposition method: a review, *BioNanoScience* 12, 1032-1057. https://doi.org/10.1007/s12668-022-00996-w

Hasan S. (2015). A review on nanoparticles: their synthesis and types. *Res J Recent Sci.* 2277, 2502.

Hossain N., Mobarak M. H., Mimona M. A., Islam M. A., Hossain A., Zohura F. T., Chowdhury M. A. (2023) Advances and significances of nanoparticles in semiconductor applications – A review, *Results Eng.* 19:101347. https://doi.org/10.1016/j.rineng.2023.101347

Husaini M. (2026) The Role of Chemistry in Solving Global Scientific and Environmental Challenges: A Comprehensive Review, *J. Mater. Environ. Sci.* 17(1), 150-175.

Iribarren A., Durán-Sosa I., González-Hurtado M., Herrera-Salvador M., Castro-Rodríguez R. (2019) Elucidating room-temperature optical transitions in annealed ZnO nanoparticles synthesized from an aqueous method, *Mater. Res. Express* 6, 105048. https://doi.org/10.1088/2053-1591/ab3865

Iribarren A., Hernández-Rodríguez E., Maqueira L. (2014) Structural, chemical and optical evaluation of Cu-doped ZnO nanoparticles synthesized by an aqueous solution method, *Mater. Res. Bull.* 60, 376–81. http://dx.doi.org/10.1016/j.materresbull.2014.08.059

Islam S. M., Ahmed S. M., Bappy A. J., Rahman M., Rahman M., Khatun E. M., Rana P. Kuddus A., Ismail M. B. A. (2025). Nanostructured CuO, ZnO, and CuO/ZnO heterostructures via acetate-based electrodeposition: exploring their optoelectronic properties for potential energy harvesting applications, *J. Mater. Environ. Sci.* 16 (3), 451-471. https://doi.org/10.1039/D5NJ02432C

JCPDS-International Centre for Diffraction Data 2003 PCPDFWIN v. 2.4 Chart No. 890510.

Jiang Z., Liu B., Yu L., Tong Y., Yan M., Zhang R. (2023) Research progresses in preparation methods and applications of zinc oxide nanoparticles, *J. Alloys Compd*. 956, 170316. https://doi.org/10.1016/j.jallcom.2023.170316

Kolahalam L. A., Viswanath I. K., Diwakar B. S., Govindh B., Reddy V., Murthy Y. L. N. (2019). Review on nanomaterials: Synthesis and applications, *Mater. Today: Proc*. 18, 2182-2190. https://doi.org/10.1016/j.matpr.2019.07.371

Leung Y. H., Djurišič A. B., Choy W. C. H., Chan W. K., Cheah K. W. (2004) ZnO nanostructures prepared by different methods, *MRS Online Proc. Library* 818, 347-352. https://doi.org/10.1557/PROC-818-M8.19.1

Malik S., Muhammad V., Waheed Y. (2023) Nanotechnology: A Revolution in Modern Industry, *Molecules* 28, 661. https://doi.org/10.3390/molecules28020661

Mittemeijer E. J., Welzel U. (2013) *Modern Diffraction Methods*. Weinheim, Germany: Wiley-VCH Verlag&Co. KGaA.

Mohammed H., Mia M. F., Wiggins J., Desai S., (2025) Nanomaterials for Energy Storage Systems—A Review, *Molecules* 30(4), 883. https://doi.org/10.3390/molecules30040883

Morkoç H., Özgür Ü. (2009) *Zinc Oxide: Fundamentals, Materials and Device Technology*. Weinheim: Wiley-VCH VerlagGmbH& Co. KGaA.

Ong C. B., Ng L. Y., Mohammad A. W. (2018) A review of ZnO nanoparticles as solar photocatalysts: synthesis, mechanisms and applications. *Renew. Sustain. Energy Rev.* 81, 536–51. https://doi.org/10.1016/j.rser.2017.08.020

Ragu Prasath A., Selvam K. A (2026) Review of the Zinc Oxide Nanoparticles Synthesis and Their Emerging Biomedical Potential. *Biomedical Materials & Devices* 4, 2832–2856. https://doi.org/10.1007/s44174-025-00422

Roduner E. (2006) Size matters: why nanomaterials are different, *Chem. Soc. Rev.* 35, 583–592. https://doi.org/10.1039/B502142C

Saeed M., Marwani H. M., Shahzad U., Asiri A. M., Rahman M. M. (2023) Recent Advances, Challenges, and Future Perspectives of ZnO Nanostructure Materials Towards Energy Applications, *Chem. Rec.* e202300106. https://doi.org/10.1002/tcr.202300106

Saidi N., Azzaoui K., Ramdani M., Mejdoubi E., Jaradat N., Jodeh S., *et al.* (2022). Design of Nanohydroxyapatite/Pectin Composite from Opuntia Ficus-Indica Cladodes for the Management of Microbial Infections. *Polymers*, 14, 14, 4446. https://doi.org/10.3390/polym14204446

Salem S. S., Hammad E. N., Mohamed A. A., El-Dougdoug W. (2022) A Comprehensive Review of Nanomaterials: Types, Synthesis, Characterization, and Applications, *Biointerface Res. Appl. Chem*. 13, 41. https://doi.org/10.33263/briac131.041

Shaba E. Y., Jacob J. O., Tijani J. O., Suleiman M. A. T. (2021) A critical review of synthesis parameters afecting the properties of zinc oxide nanoparticle and its application in wastewater treatment, *Appl. Water Sci.* 11, 48. https://doi.org/10.1007/s13201-021-01370-z

Soli J., Kachbouri S., Elaloui E., Charnay C. (2021) Role of surfactant type on morphological, textural, optical, and photocatalytic properties of ZnO nanoparticles obtained by modified sol–gel, *J. Sol-Gel Sci. Techn.* 100, 271-285. https://doi.org/10.1007/s10971-021-05653-4

Stokes R., Wilson A. J. C. (1944) The diffraction of X rays by distorted crystal aggregates – I, *Proc. Phys. Soc.* 56, 174-181. https://doi.org/10.1088/0959-5309/56/3/303

Tabaght, F. E., Azzaoui, K., Elidrissi, A., Hamed, O., Mejdoubi, E., Jodeh, S., … Lamhamdi, A. (2021). New nanostructure based on hydroxyapatite modified cellulose for bone substitute, synthesis, and characterization. *International Journal of Polymeric Materials and Polymeric Biomaterials*, 70(6), 437–448. https://doi.org/10.1080/00914037.2020.1725758

Wang Z.L. (2009) Ten years'venturing in ZnO nanostructures: from discovery to scientific understanding and to technology applications, *Chinese Sci. Bull.* 54, 4021. https://doi.org/10.1007/s11434-009-0456-0

Williamson G. K., Hall W. H. (1953) X-ray line broadening from filed aluminium and wolfram, *Acta Metall.* 1, 22–31. https://doi.org/10.1016/0001-6160(53)90006-6

Xiong L., Fu Y., Luo Y., Wei Y., Zhang Z., Wu C., Luo S., Wang G., Sawtell D., Xie K., Wu T., Ding D., Huang L. (2022) Prospective applications of transition metal-based nanomaterials. *J. Mater. Res.* 37, 2109-2123. https://doi.org/10.1557/s43578-022-00648-5

Zafar S., Ghafoor S., Jahan F., Aqsa, B. (2022) Review on synthesis and applications of nanomaterials, *SBK J. Basic Sci. and Innov. Res.* 2, 36-53.